

## RESEARCH ARTICLE

# Nanoalkalinecellulose immobilized on magnetic nanoparticles as a green catalyst for the synthesis of tetrahydrodipyrzoloxyridines and mechanistic insights under base catalysis

Fatemeh Tamaddon<sup>1</sup>  | Ehsan Ahmadi-AhmadAbadi<sup>1</sup>  | Hossein Kargar<sup>2</sup> 

<sup>1</sup>Department of Chemistry, Yazd University, Yazd, Iran

<sup>2</sup>Department of Biomedical Engineering, Meybod University, Meybod, Iran

## Correspondence

Fatemeh Tamaddon, Department of Chemistry, Yazd University, Yazd 89195-741, Iran.  
Email: ftamaddon@yazd.ac.ir

## Funding information

Yazd University Research Council

## Abstract

The cotton-derived nanoalkalinecellulose (NAC) flocculated on the Fe<sub>3</sub>O<sub>4</sub>-nanoparticles was analytically characterized as Fe<sub>3</sub>O<sub>4</sub>@NAC. With the 1:5.7 weight ratio for organic:inorganic and the base-capacity equal to 7.5 mmol HO<sup>-</sup>/g, the Fe<sub>3</sub>O<sub>4</sub>@NAC represented a catalytic advantage in the room-temperature one-pot *pseudo*-multicomponent synthesis of tetrahydrodipyrzoloxyridines (THDPPs) in water. Mechanistic monitoring supported no requisite to acid/base catalyst in the first phase for rapid formation of intermediate 3-methylpyrazolone (**A**) by Knorr reaction of the ethylacetoacetate with hydrazine hydrate in water at room temperature. Alternatively, Fe<sub>3</sub>O<sub>4</sub>@NAC showed catalytic roles in the further reaction phases in synthesis of THDPPs from the **A**. Excellent base capacity, hydrogen-bonding performance, and stability due to no significant activity loss and leaching after five reaction cycles are advantages of this organometallic catalyst.

## KEYWORDS

3-methylpyrazolone, Fe<sub>3</sub>O<sub>4</sub>@nanoalkalinecellulose, magnetic base catalyst, tetrahydrodipyrzoloxyridines

## 1 | INTRODUCTION

Functionalized magnetic nanoparticles (FMNs) by biopolymers are advanced nano-biomaterials<sup>[1–5]</sup> with cooperative synergistic effects to resolve either agglomeration issues of MNs or separation problems of biopolymers.<sup>[6–8]</sup> Microcellulose (MC) and nanocellulose (NC) are among the best biopolymers applied for improving the dispersion of magnetite (Fe<sub>3</sub>O<sub>4</sub>) and maghemite-based FMNs.<sup>[9–11]</sup> Despite the performances of Fe<sub>3</sub>O<sub>4</sub><sup>[12–14]</sup> and

MC/NC,<sup>[15–18]</sup> linking of them in FMNs needs higher energy than hydrogen bonding and thermal stability than cellulose at 70°C.<sup>[2,19]</sup> Consequently, higher stable and negatively charged micro-/nano-alkaline celluloses (MAC/NAC) are superior to native MC/NC due to their strong electrostatic interactions with FMNs. Recently, we have developed anionic carbohydrate polymers including MAC/NAC,<sup>[20]</sup> anionic cellulose,<sup>[21]</sup> alkaline starch,<sup>[22]</sup> and anionic NC<sup>[23]</sup> with some filtration/centrifugation issues for recycling. To solve these disputes,

This work is fully related to the PhD dissertation of Ehsan Ahmadi-AhmadAbadi. The authors are also not employed by a nonacademic government agency that has a primary function other than research and/or education and thus are not submitting this manuscript as an official representative or on behalf of the government. The authors and reviewers do not have any conflict of interest as per the COPE Guidelines.

immobilization of anionic-NAC on the nanoFe<sub>3</sub>O<sub>4</sub> by flocculation is anticipated to give a new magnetically recoverable base and organic–inorganic hybrid catalyst.

*Tetra*-hydrodipyrzoloypyridines (THDPPs) are attractive fused heterocyclic compounds because of their electroluminescence properties in polymer systems<sup>[24]</sup> and the pharmaceutical role of the pyrazolopyridine in zaleplon, indiplon, etazolate, and cartazolate drugs.<sup>[25]</sup> Although the first synthesis of THDPPs is a Hantzsch<sup>[26]</sup>-type *pseudo*-multicomponent reaction (*p*-MCR) directed by Zhao et al.,<sup>[27]</sup> a recently modified acid-catalyzed *p*-MCR of hydrazine, ethyl acetoacetate, ammonium acetate, and aldehyde (2:2:1:1) has been developed for the synthesis of THDPPs.<sup>[28–31]</sup> We have also settled synthesis of THDPPs in water using new DESs or nonhygroscopic nitrogen sources,<sup>[31–33]</sup> although all acid-catalyzed protocols emphasized the 3-methylpyrazolone (**A**) as the reaction intermediate. However, no detail is available for the less hazardous heterogeneous base-catalyzed synthesis of THDPPs. Herein, for the first time, the magnetic base catalyst Fe<sub>3</sub>O<sub>4</sub>@NAC was prepared by the immobilization of cotton-derived NAC on Fe<sub>3</sub>O<sub>4</sub>-MNPs, and the catalytic activity of this novel core-shell catalyst investigated in the very rapid *p*-MC synthesis of THDPPs in water at room temperature. After some mechanistic insights for this base-catalysis synthesis, the intermediate **A** was rapidly prepared and balanced in a very fast Fe<sub>3</sub>O<sub>4</sub>@NAC-catalyzed *p*-MCR for the THDPPs synthesis. The excellent stability of this heterogeneous, organic–inorganic hybrid, reusable, and magnetic base catalyst was confirmed by different techniques to support its catalytic performance.

## 2 | MATERIALS AND METHODS

### 2.1 | General

All chemicals were purchased from Merck and Sigma without further purification. All yields refer to isolated products, which were characterized by spectral data. The Fourier transform infrared (FT-IR) spectra were recorded on a Bruker spectrophotometer as KBr disks. Melting points were determined by a Buchi B-540 apparatus. Melting points were determined by a Buchi B-540 apparatus. The vibrating sample magnetometry (VSM) of magnetic materials was monitored by the Lake Shore Cryotronics 7404 at 298 K. Field-emission scanning electron microscopy (FESEM) and transmission electron microscopy (TEM) images performed with MIRA3TESCAN-XMU. The X-ray diffraction (XRD) and thermal gravimetric analysis (TGA) were recorded with PHILIPS PW1730 and TGA-TA Q600, respectively. The

leaching test for iron ions was evaluated by inductively coupled plasma mass spectrometry (ICP-MS) analysis (PerkinElmer, 9000). The nuclear magnetic resonance (NMR) spectra were recorded in CDCl<sub>3</sub> or DMSO-*d*<sub>6</sub> on Bruker Avance NMR 400 MHz.

### 2.2 | Preparation of nanoFe<sub>3</sub>O<sub>4</sub>

To the FeCl<sub>3</sub>·6H<sub>2</sub>O (6.75 g) and FeCl<sub>2</sub>·4H<sub>2</sub>O (2.5 g) dissolved in distilled water (100 mL), NH<sub>4</sub>OH was added drop-wise within 1 h until pH 12, and the mixture was stirred for 1 h at 40°C. After completion, the nanoFe<sub>3</sub>O<sub>4</sub> was washed with water, separated by an external magnet, and dried at 50°C in an oven.

### 2.3 | Preparation of NAC solution from cotton

Prewashed cotton (1.75 g) was added to a mixture of urea (4.0 g), sodium hydroxide (4.0 g), and thiourea (2.3 g) in distilled water (40 mL); the resulting suspension maintained at cold thermal shock (−12°C) for 6 h<sup>[21]</sup>; and the final mixture stirred vigorously at room temperature to obtain NAC solution.

### 2.4 | Immobilization of NAC on Fe<sub>3</sub>O<sub>4</sub> as Fe<sub>3</sub>O<sub>4</sub>@NAC core-shell

To the dispersed mixture of nanoFe<sub>3</sub>O<sub>4</sub> (1.75 g) in the above NAC solution, ammonium sulfate (2.86 g) was added as a flocculating agent, and the suspension was stirred vigorously for 6 h at 50°C. Then water and acetone were added and decanted until removing free NaOH and urea from the magnetically separated Fe<sub>3</sub>O<sub>4</sub>@NAC that dried at 50°C.

### 2.5 | Base capacity of Fe<sub>3</sub>O<sub>4</sub>@NAC

The dispersed Fe<sub>3</sub>O<sub>4</sub>@NAC (0.1 g) in distilled water (20 mL) was titrated with standard HCl (0.22 M) using the indicator bromtimol-blue to reach the end point.

### 2.6 | Synthesis and characterization of 3-methylpyrazolone (**A**)

A mixture of hydrazine hydrate (2.0 mmol) and ethyl acetoacetate (2.0 mmol) in water (1.0 mL) was stirred at room temperature for 5 min without or with the

catalyst Fe<sub>3</sub>O<sub>4</sub>@NAC (12 mg). In the latter case, the catalyst was collected by a magnet, and the precipitated product in water was rapidly filtered, washed, with water/hexane, and dried to yield 97% A as a white solid with mp = 222–224 °C,<sup>[34]</sup> which then identified by its FT-IR spectrum.

## 2.7 | General method for the Fe<sub>3</sub>O<sub>4</sub>@NAC-catalyzed synthesis of THDPPs

For the *p*-MC synthesis of THDPPs from hydrazine hydrate, Fe<sub>3</sub>O<sub>4</sub>@NAC (12 mg) was added to the mixture of aldehyde (1.0 mmol), hydrazine hydrate (2.0 mmol), ethyl acetoacetate (2.0 mmol), and anhydrous NH<sub>4</sub>OAc (1.0 mmol) in water (0.5 mL) and stirred at room temperature for ~5–15 min until the product precipitation. Then, water was added, the catalyst was collected by a magnet, and the pure THDPP product was filtered.

For the *p*-MC synthesis of THDPPs from the intermediate **A**, the mixture of Fe<sub>3</sub>O<sub>4</sub>@NAC (12 mg), aldehyde (1.0 mmol), the as-prepared **A** (2.0 mmol), and anhydrous NH<sub>4</sub>OAc (1.0 mmol) in water (0.5 mL) was stirred at room temperature for ~5–15 min. Then, hot ethanol (4 mL) was added, the catalyst was collected by a magnet, and the pure THDPP was isolated after the addition of cold water and filtration.

## 2.8 | Representative characterization data for the selected products

Although spectroscopic spectra (FT-IR, <sup>1</sup>H NMR, and <sup>13</sup>C NMR) for all final products (THDPP1–9) are presented in Figures S1–S24), the characteristic data for the selected products are designated below.

### 2.8.1 | 3,5-Dimethyl-4-(phenyl)-1,4,7,8-tetrahydrodipyrzolo[3,4-b, 4',3'-e] pyridine (THDPP1)

Yield: 97%; white solid, mp = 240–242 °C. FT-IR (KBr): 3410 (NH stretching), 2983, 2922 (CH stretching), 1605 (C=N stretching), 1497, 1448 (CH bending), 1368 (Methyl-CH bending) cm<sup>-1</sup>. <sup>1</sup>H NMR (400 MHz, DMSO-*d*<sub>6</sub>): δ = 2.04 (s, 6H, 2 CH<sub>3</sub>), 4.79 (s, 1 H, CH), 7.10–7.20 (3 H, ortho and para H<sub>s</sub>), 7.20–7.25 (2 H, meta H<sub>s</sub>), 11.34 (s, 3 H, 3 NH) ppm. <sup>13</sup>C NMR (100 MHz, DMSO-*d*<sub>6</sub>): δ = 12.1, 38.2, 104.8, 127.1, 128.7, 128.9, 141.0, 143.7, 145.5 ppm (Figures S1–S3).

### 2.8.2 | 3,5-Dimethyl-4-(4-*N,N*-methyl-phenyl)-1,4,7,8-tetrahydrodipyrzolo[3,4-b, 4',3'-e] pyridine (THDPP2)

Yield: 97%; yellow-orange solid, mp = 250–252 °C. FT-IR (KBr): 3514, 3168 (NH stretching), 2942 (CH stretching), 1608 (C=N stretching), 1520 (C=C aromatic), 1139 (C–N stretching) cm<sup>-1</sup>. <sup>1</sup>H NMR (400 MHz, DMSO-*d*<sub>6</sub>): δ = 2.26 (s, 6H, 2 CH<sub>3</sub>), 2.91 (s, 6H, 2 CH<sub>3</sub> [para]), 4.9 (s, 1 H, CH), 6.75 (d, *J* = 8 Hz, 2H, H<sub>arom</sub>), 7.3 (d, *J* = 8 Hz, 2H, H<sub>arom</sub>), 4.07 (s, 1H, NH) 11.54 (s, 2H, 2 NH) ppm (Figures S4–S6).

### 2.8.3 | 3,5-Dimethyl-4-(4-methyl-phenyl)-1,4,7,8-tetrahydrodipyrzolo[3,4-b, 4',3'-e] pyridine (THDPP3)

Yield: 94%; white solid, mp = 244–246 °C. FT-IR (KBr): 3170 (NH stretching), 2920 (CH stretching), 1610 (C=N stretching), 1520 (C=C aromatic), 1139 (C–N stretching) cm<sup>-1</sup>. <sup>1</sup>H NMR (400 MHz, DMSO-*d*<sub>6</sub>): δ = 2.1 (s, 6H, 2 CH<sub>3</sub>), 2.20 (s, 3 H, CH<sub>3</sub> [para]), 4.78 (s, 1 H, CH), 6.99–7.00 (m, 4H, H<sub>arom</sub>), 11.25 (s, 3 H, 3 NH) ppm. <sup>13</sup>C NMR (100 MHz, DMSO-*d*<sub>6</sub>): δ = 10.85, 20.98, 32.85, 104.85, 127.82, 128.83, 134.70, 140.20, 140.75, 161.50 ppm (Figures S7–S9).

### 2.8.4 | 3,5-Dimethyl-4-(4-hydroxy-phenyl)-1,4,7,8-tetrahydrodipyrzolo[3,4-b, 4',3'-e] pyridine (THDPP7)

Yield: 93%; white solid, mp = 267–269 °C. FT-IR (KBr): 3234 (overlapped NH and OH stretching), 2,935 (CH stretching), 1600 (C=N stretching), cm<sup>-1</sup>. <sup>1</sup>H NMR (400 MHz, DMSO-*d*<sub>6</sub>): δ = 2.05 (s, 6H, 2 CH<sub>3</sub>), 4.68 (s, 1 H, CH), 6.57 (d, *J* = 8 Hz, 2 H, H<sub>arom</sub>), 6.89 (d, *J* = 8 Hz, 2 H, H<sub>arom</sub>), 9.15 (s, OH), 11.52 (s, 3 H, 3 NH) ppm. <sup>13</sup>C NMR (100 MHz, DMSO-*d*<sub>6</sub>): δ = 10.35, 31.76, 104.51, 114.45, 128.25, 133.36, 139.75, 155.05, 161.05 ppm (Figures S17–S19).

### 2.8.5 | 3,5-Dimethyl-4-(4-nitro-phenyl)-1,4,7,8-tetrahydrodipyrzolo[3,4-b, 4',3'-e] pyridine (THDPP8)

Yield: 96%; cream solid, mp = 333–335 °C. FT-IR (KBr): 3250 (NH stretching), 2985 (CH stretching), 1605 (C=N stretching), 1489 (asymmetrical stretching NO<sub>2</sub> overlapped with the C=C aromatic), 1352 (NO<sub>2</sub> symmetrical stretching), 753 (out of plane bending C–H, para-

substituted)  $\text{cm}^{-1}$ .  $^1\text{H}$  NMR (400 MHz,  $\text{DMSO-}d_6$ ):  $\delta = 2.1$  (s, 6 H, 2  $\text{CH}_3$ ), 4.95 (s, 1H, CH), 7.35 (d,  $J = 8$  Hz, 2 H,  $\text{H}_{\text{arom}}$ ), 8.1 (d,  $J = 8$  Hz, 2 H,  $\text{H}_{\text{arom}}$ ), 11.20 (s, 3H, 3 NH) ppm.  $^{13}\text{C}$  NMR (100 MHz,  $\text{DMSO-}d_6$ ):  $\delta = 10.70, 33.40, 103.60, 123.40, 129.20, 140.20, 146.1, 152.25, 161.35$  ppm (Figures S20–S22).

## 2.9 | Metal leaching, recycling, and reusing of the catalyst

Owing to the insolubility of catalyst in water, it was separated by a magnet after the model reaction completion for synthesis of THDDP1, washed with acetone, dried at  $50^\circ\text{C}$ , and reused in further reaction runs. The leaching test for entering the  $\text{Fe}^{+2}/\text{Fe}^{+3}$  to reaction mixture was evaluated for the fresh and reused filtrate solutions of  $\text{Fe}_3\text{O}_4@\text{NAC}$  after fourth cycle by ICP-mass analysis.

## 3 | RESULTS AND DISCUSSION

### 3.1 | Preparation of $\text{Fe}_3\text{O}_4@\text{NAC}$

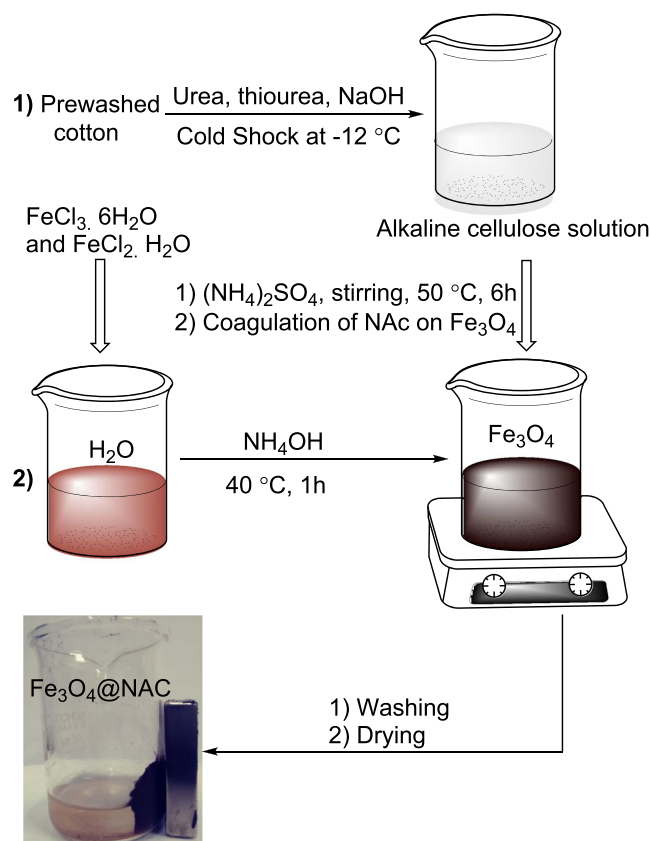
Initially, NAC suspension was prepared by urea/thiourea/NaOH treatment of the cotton-derived MC and additional freezing shock at  $-12^\circ\text{C}$ .<sup>[21–23]</sup> Further coagulation of NAC on the prepared  $\text{Fe}_3\text{O}_4$  nanoparticles led to the  $\text{Fe}_3\text{O}_4@\text{NAC}$ , although salting-out effect by ammonium sulfate and alkali washing provided maximum uniformity of flocculated NAC-shell and basicity preservation of core-shell (Scheme 1).

### 3.2 | Characterization results of $\text{Fe}_3\text{O}_4@\text{NAC}$

The structure of the  $\text{Fe}_3\text{O}_4@\text{NAC}$  was identified by base capacity, FT-IR, XRD, FESEM, TEM, VSM, TGA, and Brunauer–Emmett–Teller (BET) analyses. According to the consumed standard HCl in the acid–base titration, the base capacity of the  $\text{Fe}_3\text{O}_4@\text{NAC}$  was determined as 7.5 mmol  $\text{HO}^-/\text{g}$ , which is significantly higher than either neutral  $\text{Fe}_3\text{O}_4$  or NC. This high basicity matches with the created alkoxide groups by alkalizing of some aggregate hydrogen-bonded NAC-OHs in the outer shell of  $\text{Fe}_3\text{O}_4@\text{NAC}$ .

#### 3.2.1 | Fourier transform infrared spectra

The overlaid FT-IR spectra of the  $\text{nanoFe}_3\text{O}_4$ , NAC, and  $\text{Fe}_3\text{O}_4@\text{NAC}$  show the broad absorption bands at



**SCHEME 1** Preparation of magnetic base catalyst  $\text{Fe}_3\text{O}_4@\text{NAC}$

$\sim 2800\text{--}3600$  and  $585\text{ cm}^{-1}$  related to the surface OHs and Fe/O vibration modes in the spectrum of  $\text{nanoFe}_3\text{O}_4$ . The weak and broad absorption bands for O–H stretching at  $2500\text{--}3600\text{ cm}^{-1}$  besides to C–H stretching,  $\text{CH}_2$  bending, and C–O stretching modes at 2890, 1424, and  $1018\text{ cm}^{-1}$  in the spectrum of NAC confirmed its structure. In the FT-IR spectrum of  $\text{Fe}_3\text{O}_4@\text{NAC}$ , shifted broad absorption bands to 3400–3600, 2922, 1455, and  $1021\text{ cm}^{-1}$  attribute to the coating of  $\text{Fe}_3\text{O}_4$  nanoparticles by NAC (Figure 1).

#### 3.2.2 | X-ray diffraction

In the overlaid XRD patterns for the  $\text{Fe}_3\text{O}_4$  and  $\text{Fe}_3\text{O}_4@\text{NAC}$ , the six sharp characteristic peaks at  $2\theta = 30.81^\circ, 36.04^\circ, 43.78^\circ, 54.00^\circ, 54.10^\circ,$  and  $63.28^\circ$ , correspond to (220), (311), (400), (511), (422), and (440) planes, are compatible with the standard  $\text{Fe}_3\text{O}_4$ -phase (JCPDS card no. 39-1346). Repeating these planes as slightly broader peaks in the  $\text{Fe}_3\text{O}_4@\text{NAC}$  phase reveals conserving the  $\text{Fe}_3\text{O}_4$ -crystalline phase in this core-shell (Figure 2). Such low phase transformation with the appearance of new broad peaks at  $2\theta = 20\text{--}25^\circ$  in XRD pattern of  $\text{Fe}_3\text{O}_4@\text{NAC}$  due to crystalline cellulose

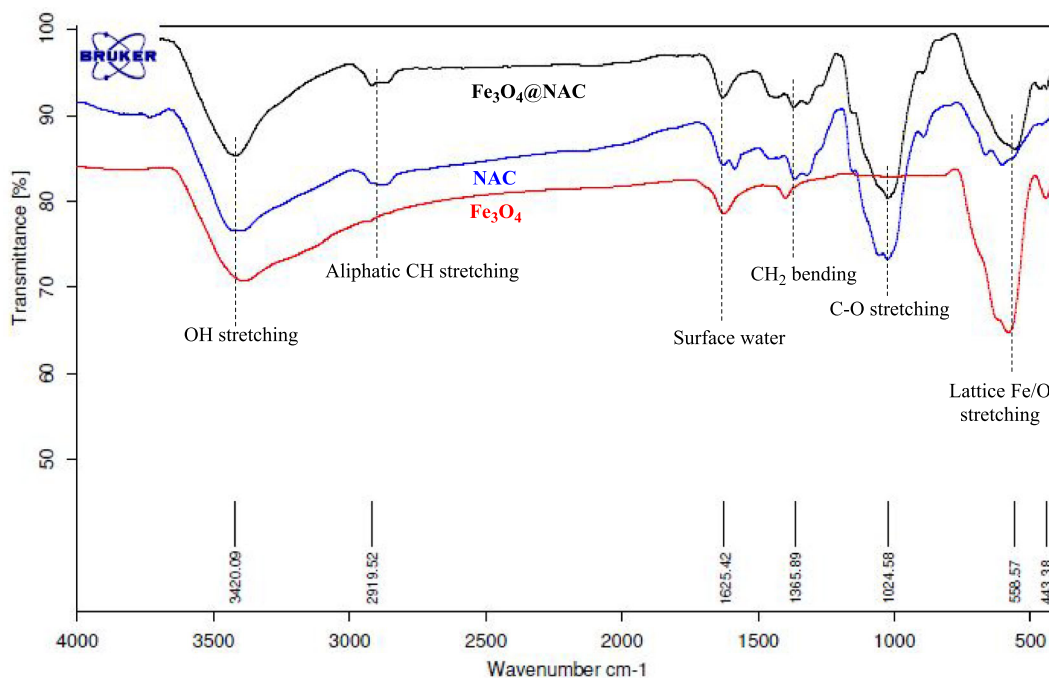
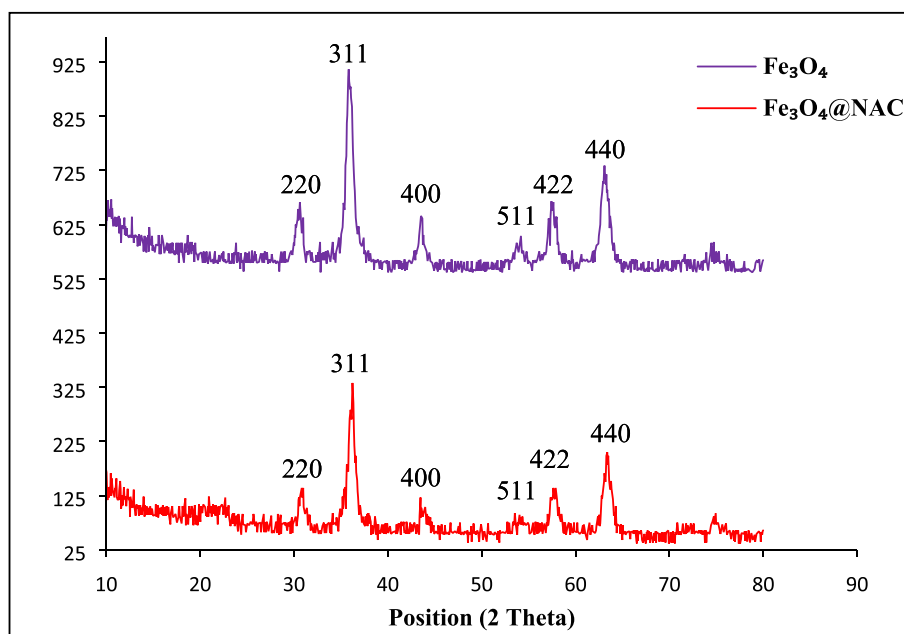


FIGURE 1 The Fourier transform infrared (FT-IR) spectra of nanoFe<sub>3</sub>O<sub>4</sub>, nanoalkalinecellulose (NAC), and Fe<sub>3</sub>O<sub>4</sub>@NAC

FIGURE 2 X-ray diffraction (XRD) patterns of nanoFe<sub>3</sub>O<sub>4</sub> and Fe<sub>3</sub>O<sub>4</sub>@NAC



showed tiny immobilization of NAC on the Fe<sub>3</sub>O<sub>4</sub>, which is further confirmed by TEM and TGA analyses.

### 3.2.3 | Field scanning electron microscopy

The comparative FESEM images of Fe<sub>3</sub>O<sub>4</sub> and Fe<sub>3</sub>O<sub>4</sub>@NAC (Figure 3) show different surface morphologies and size distribution for the spherical agglomerated Fe<sub>3</sub>O<sub>4</sub> nanoparticles from 22–36 nm to slightly larger dispersed Fe<sub>3</sub>O<sub>4</sub>@NAC nanospheres with 25- to 38-nm

diameter. This slight enlargement is due to a thin layer immobilization of NAC on nanoFe<sub>3</sub>O<sub>4</sub>-particles in Fe<sub>3</sub>O<sub>4</sub>@NAC that improved the nanoparticles agglomeration and surface roughness (Figure 3, right).

### 3.2.4 | TEM and histogram of Fe<sub>3</sub>O<sub>4</sub>@NAC nanoparticles

While the TEM of Fe<sub>3</sub>O<sub>4</sub>@NAC (Figure 4, left) shows the well-defined coating of the Fe<sub>3</sub>O<sub>4</sub> nanospheres by NAC,

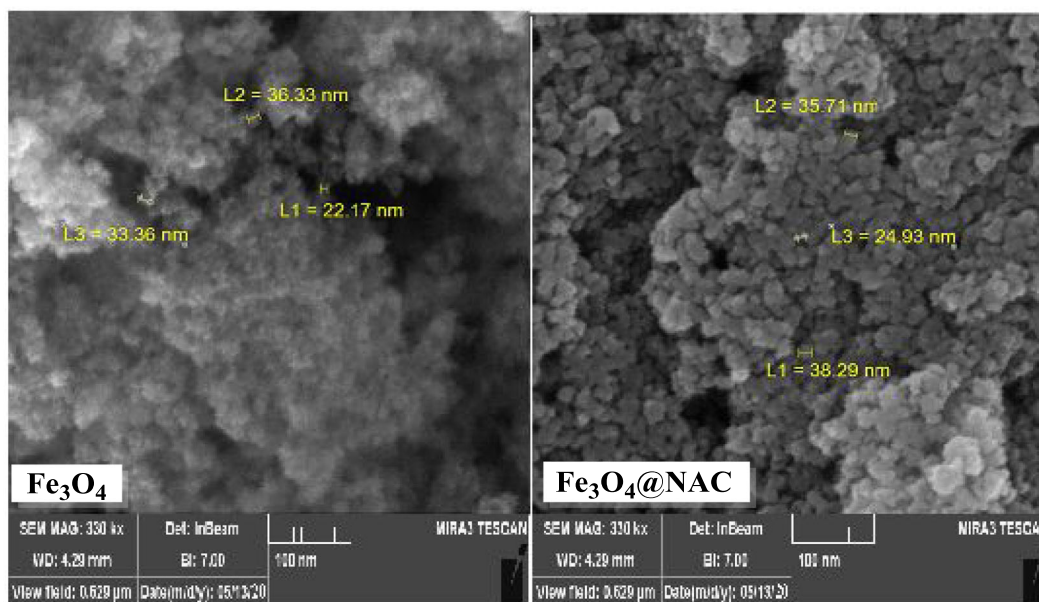


FIGURE 3 Field-emission scanning electron microscopy (FESEM) images of nano $\text{Fe}_3\text{O}_4$  and nano $\text{Fe}_3\text{O}_4$ @NAC

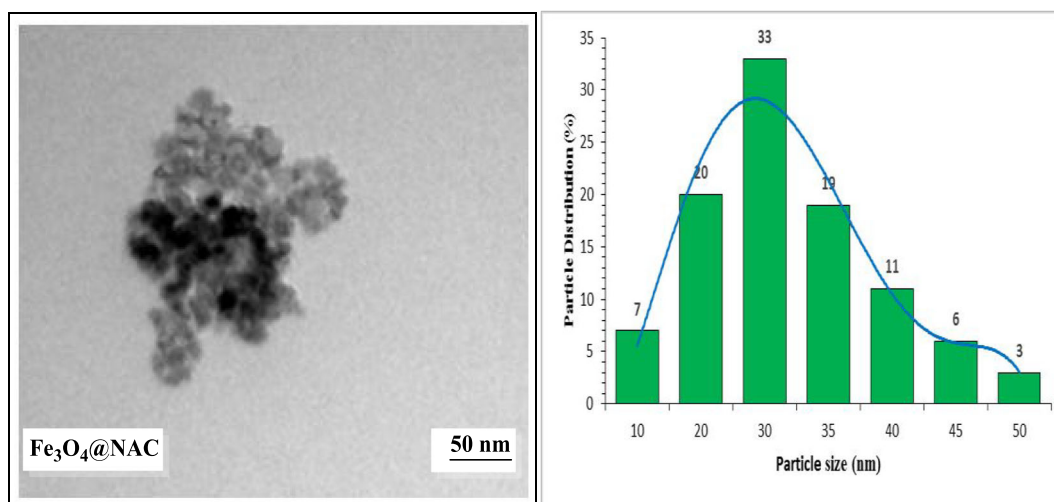


FIGURE 4 Transmission electron microscopy (TEM) image (left) and histogram of  $\text{Fe}_3\text{O}_4$ @NAC nanoparticles (right)

the histogram of the size distribution versus the particle size, detected by MIRA3TESCAN software in FESEM and TEM analyses, showed an average size of 20–35 nm for these core–shell nanoparticles (Figure 4, right).

### 3.2.5 | VSM, TGA, and BET analyses of $\text{Fe}_3\text{O}_4$ @NAC

VSM curves of bare and NAC-coated nano $\text{Fe}_3\text{O}_4$  show a decrease in magnetization saturation ( $M_s$ ) from 69.2 to 35.2  $\text{emu g}^{-1}$  (Figure 5, left). Such decrease in  $M_s$  is another evidence for  $\text{Fe}_3\text{O}_4$  coating by a nonmagnetic

layer of NAC in the super-paramagnetic core–shell of  $\text{Fe}_3\text{O}_4$ @NAC. Besides, the three times higher  $M_s$ , remanence ( $M_R$ ), and coercivity ( $H_C$ ) of the  $\text{Fe}_3\text{O}_4$ @NAC (35.2  $\text{emu g}^{-1}$ , 1.86  $\text{emu g}^{-1}$ , and 66.23 Oe) than a previously prepared MC composite<sup>[14]</sup> approve the proficiencies of the nanosizing and surface charge of NAC in these improved FMNs.  $\text{Fe}_3\text{O}_4$ @NAC is an anionic core–shell with the excellent magnetic response to an external magnet.

Comparing the thermal behaviors of the  $\text{Fe}_3\text{O}_4$ @NAC and  $\text{Fe}_3\text{O}_4$  by TGA in air shows respective 2% and 19% weight losses at  $<500^\circ\text{C}$  and defines 17% NAC sorption on  $\text{Fe}_3\text{O}_4$  equal to 1:5.7 weight ratio for the anionic

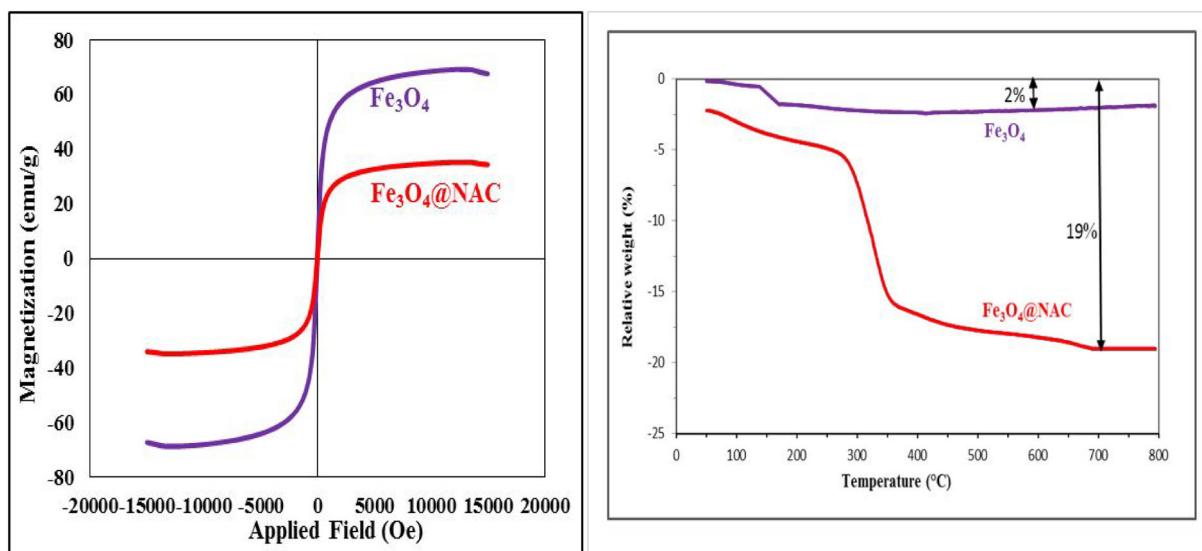
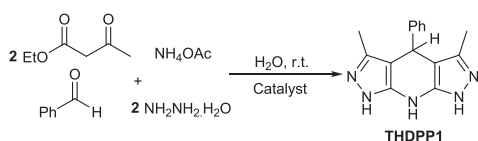


FIGURE 5 Comparative vibrating sample magnetometries (VSMs) (left) and thermal gravimetric analyses (TGAs) of Fe<sub>3</sub>O<sub>4</sub> and Fe<sub>3</sub>O<sub>4</sub>@NAC (right)



SCHEME 2 The typical *pseudo*-multicomponent reaction (*p*-MCR) for THDPP1 synthesis

organic shell versus the inorganic magnetic core. The break-in weight loss at  $\sim 300^\circ\text{C}$  for Fe<sub>3</sub>O<sub>4</sub>@NAC is attributed to the NAC-glucose-unit decomposition (Figure 5, right).

Based on the BET analysis, the specific surface area, total pore volume, and mean pore diameter for nanoFe<sub>3</sub>O<sub>4</sub> dramatically decreased from 90.90 m<sup>2</sup> g<sup>-1</sup>, 0.3 cm<sup>3</sup> g<sup>-1</sup>, and 13.37 nm to 14.1 m<sup>2</sup> g<sup>-1</sup>, 0.030 cm<sup>3</sup> g<sup>-1</sup>, and 9.96 nm in nanoFe<sub>3</sub>O<sub>4</sub>@NAC. The 14 times higher

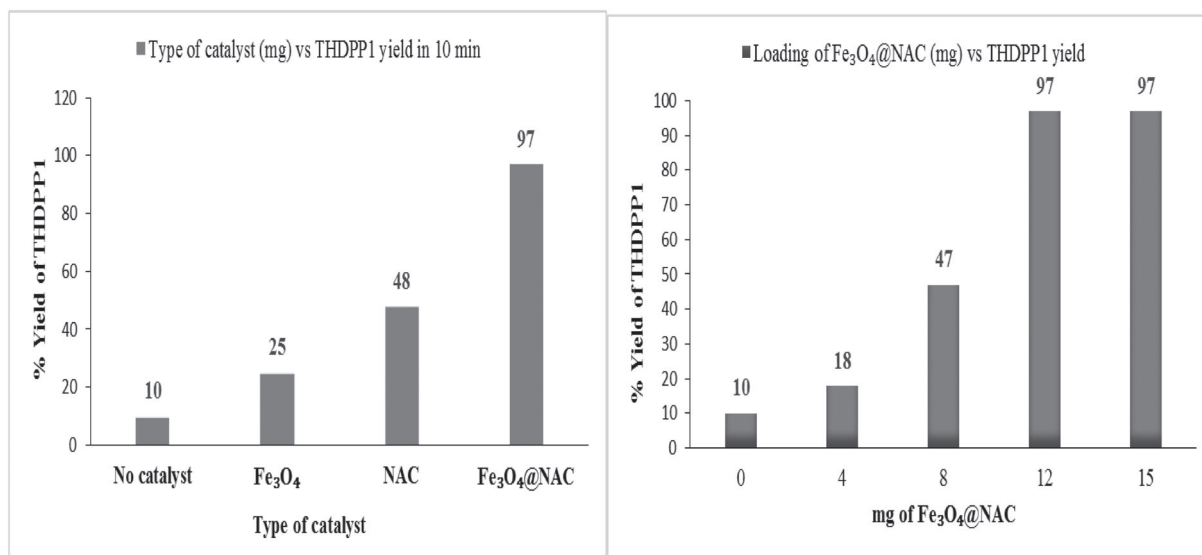


FIGURE 6 Optimization of catalyst and catalyst-loading for THDPP1 synthesis

and 6.5 times lower surface area of this core-shell than cotton ( $1.01 \text{ m}^2 \text{ g}^{-1}$ ) and nano $\text{Fe}_3\text{O}_4$  describes  $\text{Fe}_3\text{O}_4$  pores filling by a uniform thin layer of NAC shell in  $\text{Fe}_3\text{O}_4$ @NAC and surface improving than cotton.

### 3.3 | Catalytic valuation of $\text{Fe}_3\text{O}_4$ @NAC in the MC synthesis of THDPPs

Firstly, the catalytic efficiencies of the  $\text{Fe}_3\text{O}_4$ @NAC, free  $\text{Fe}_3\text{O}_4$ , and NAC (each 0.15 g) were compared in the typical synthesis THDPP1 by *p*-MCR of benzaldehyde,  $\text{NH}_4\text{OAc}$ , hydrazine hydrate, and ethyl acetoacetate (1:1:2:2 molar ratio) in water at room temperature (Scheme 2, Figure 6, left). With a higher superiority in yield at 10 min, THDPP1 was precipitated in 97% yield

using very low loading of  $\text{Fe}_3\text{O}_4$ @NAC (12 mg) (Figure 6, right).

Comparing the reaction yield and time for NAC and  $\text{Fe}_3\text{O}_4$ @NAC reveals that basicity is not the only factor for catalytic activity. Thus, the proficiency of this magnetically separable base catalyst is attributed to its multifunctionality and hybrid organic-inorganic nanostructure that forms a nanoporous magnetic gel in water by a hydrogen-bonded network in swelling. These properties provide multiactive sites, high diffusion power, uniformity, and well dispersion of catalyst in the aqueous medium of reaction to activate the reactants in nanopores of catalyst and directing the reaction energy path to the rapid yielding of product. The 33% decrease in the THDPP1 yield for a similar reaction in EtOH supports this interpretation (Figure 7, left). Evaluation of the

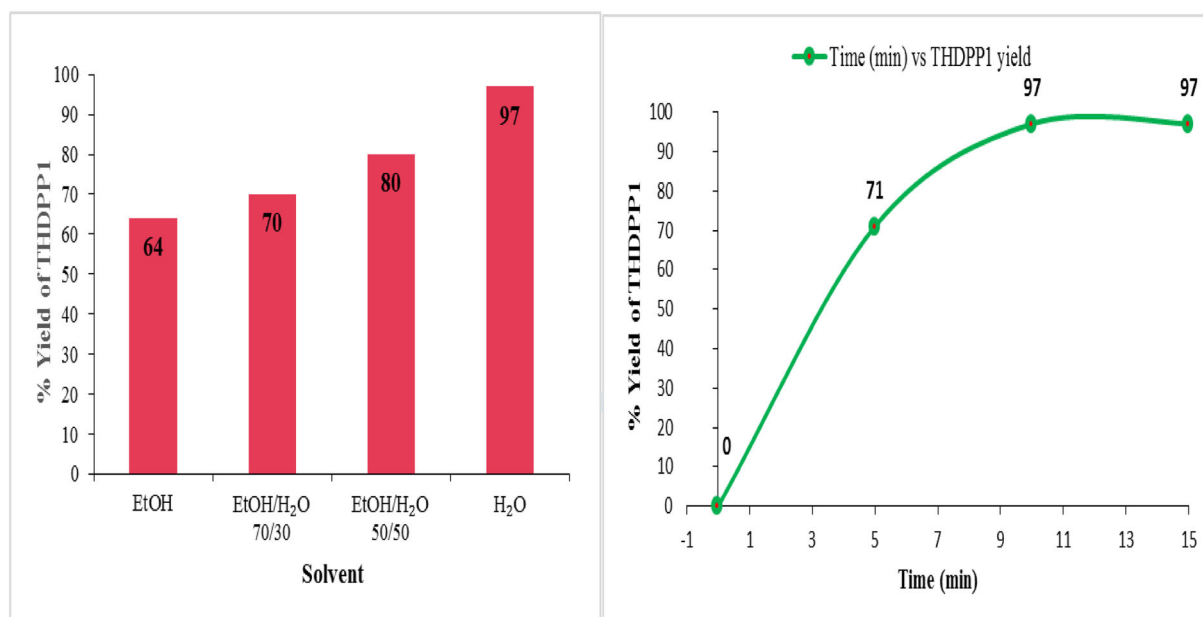


FIGURE 7 Solvent effect (left) and reaction time for the  $\text{Fe}_3\text{O}_4$ @NAC-catalyzed THDPP1 synthesis by the room temperature reaction of benzaldehyde,  $\text{NH}_4\text{OAc}$ , hydrazine hydrate, and ethyl acetoacetate (1:1:2:2) in water

TABLE 1 Comparative performances of the  $\text{Fe}_3\text{O}_4$ @NAC with the previous methods for the synthesis of THDPP1 by *p*-MCR in Scheme 2

Entry	Reaction conditions	Time (min.)	Yield (%)	Ref.
1	Choline chloride/urea, 110°C	30	92	Vanegas et al. <sup>[35]</sup>
2	Ultrasonic, H <sub>2</sub> O, 50°C	120	95	Shabalala et al. <sup>[36]</sup>
3	Pseudopolymeric nanoparticles, EtOH, r.t.	30	90	Dashteh et al. <sup>[37]</sup>
4	Reflux, EtOH	300	72	Dabiri et al. <sup>[28]</sup>
5	$\text{Fe}_3\text{O}_4$ @KCC-1-nPr-NH <sub>2</sub> , ethanol, reflux	30	92	Azizi et al. <sup>[14]</sup>
6	Co4ChDES, H <sub>2</sub> O, 60°C	15	94	Tamaddon and Khorram <sup>[31]</sup>
7	$\text{Fe}_3\text{O}_4$ @NAC, H <sub>2</sub> O, r.t.	10	97	This work

Abbreviation: *p*-MCR, pseudo-multicomponent reaction.

reaction's time impact on the THDPP1 yield using the optimized catalyst loading (12-mg  $\text{Fe}_3\text{O}_4\text{@NAC}$ ) revealed that the optimum reaction time is 10 min (Figure 7, right).

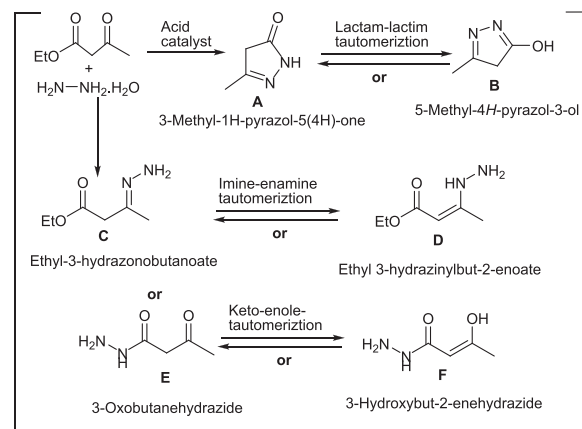
To weigh the performance of this magnetically separable base catalyst in MC synthesis of THDPP1, our results were compared with the previously reported corresponding works (Table 1) and base catalysts in water (Figure 8).

As performance results show, the organic-inorganic hybrid catalyst  $\text{Fe}_3\text{O}_4\text{@NAC}$  with advantages of simple handling and easy separation at mild conditions enhances the reaction yield and rate more efficiently than the cited previous protocols in Table 1. Besides, superiority of this magnetic base catalyst and procedure are higher than the reported homogeneous base catalysts for the same MC synthesis of THDPP1 in water<sup>[28,33,38]</sup> (Figure 8).

### 3.4 | Proposed reaction mechanism

To probe the mechanism and detailing the base-catalyzed rapid synthesis of THDPP1 using  $\text{Fe}_3\text{O}_4\text{@NAC}$ , several control experiments were performed. The comparative typical *p*-MC synthesis of THDPP1 at room temperature in the absence and presence of  $\text{Fe}_3\text{O}_4\text{@NAC}$  in water yielded only 10% and 60% THDPP1 after 10 and 60 min using no catalyst. Due to the isolation of THDPP1 in 97% yield after 10 min using only 12-mg  $\text{Fe}_3\text{O}_4\text{@NAC}$ , it has a

catalytic role in this one-pot *p*-MCR. However, the previous acid-catalyzed mechanisms for the THDPPs synthesis<sup>[29,30]</sup> proposed formation of intermediate 3-methylpyrazolone (A) by Knorr pyrazole formation in the first reaction step.<sup>[39]</sup> To clear the catalytic role of  $\text{Fe}_3\text{O}_4\text{@NAC}$  in the reaction of ethyl acetoacetate and hydrazine hydrate, the product, yield, and time were compared in this phase by a classical method,<sup>[34]</sup> a deep-eutectic catalyst at 110°C,<sup>[35]</sup> *p*-TsOH,<sup>[29]</sup>  $\text{Fe}_3\text{O}_4\text{@NAC}$ , and catalyst-free conditions in water. While the isolated product in each case was identified by FT-IR and melting point, none of the probable intermediates B–F were detected (Scheme 3).



**SCHEME 3** Possible intermediates in the reaction of hydrazine with ethyl acetoacetate

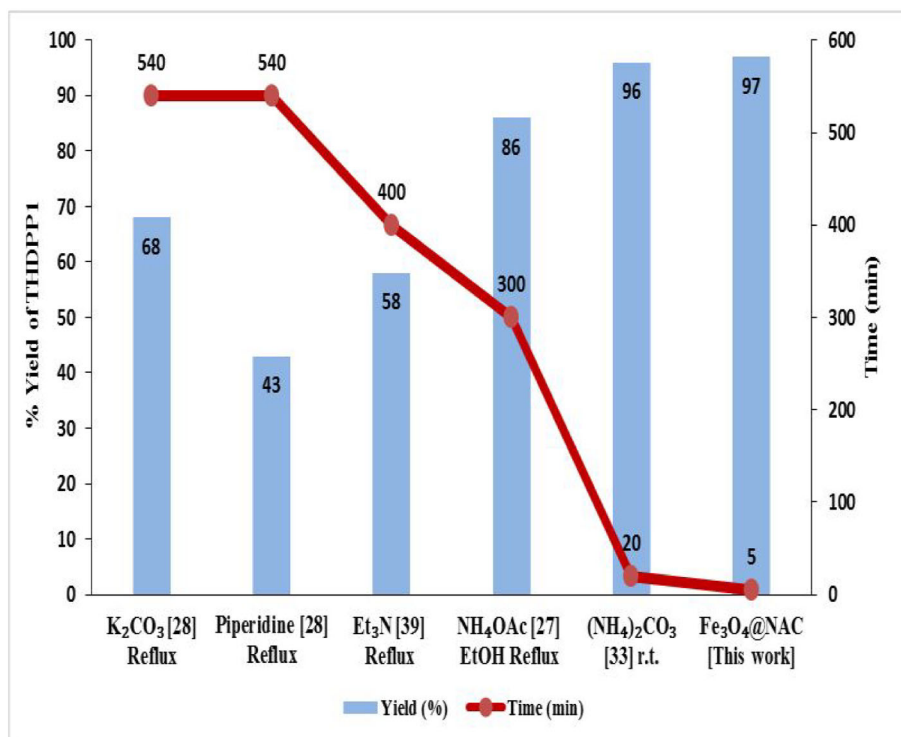


**FIGURE 8** Performance of the  $\text{Fe}_3\text{O}_4\text{@NAC}$  for the synthesis of THDPP1

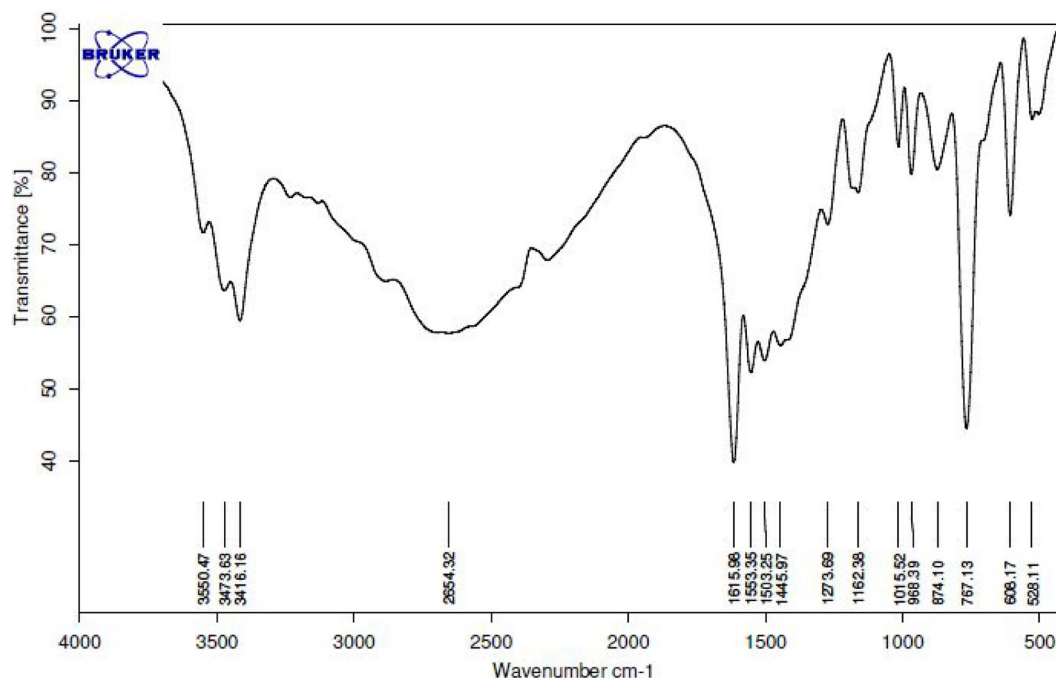
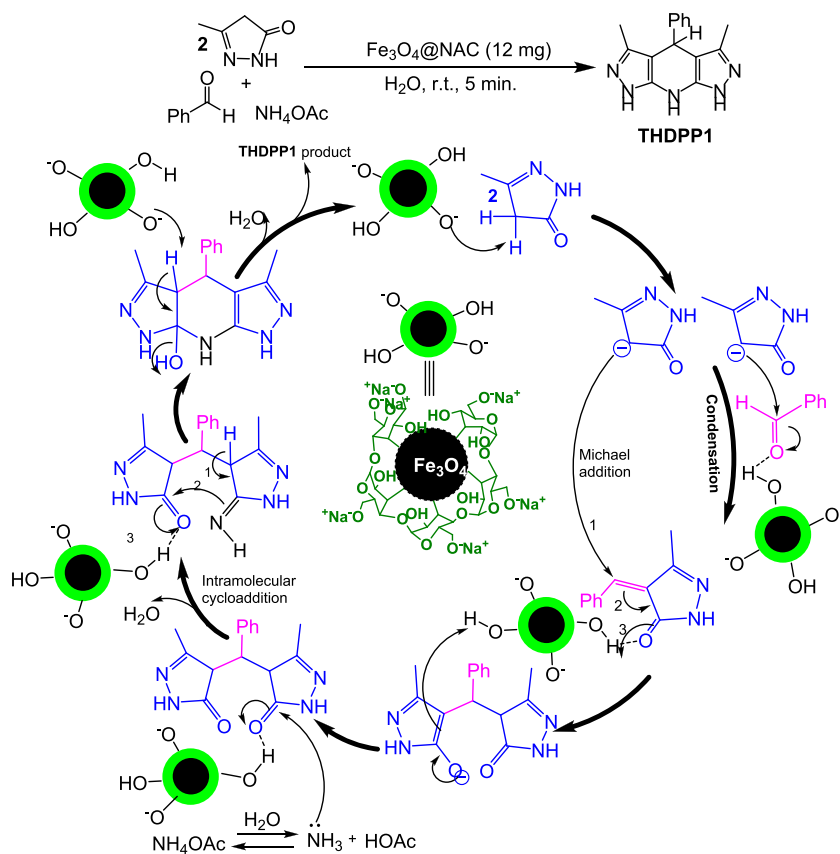


FIGURE 9 The Fourier transform infrared (FT-IR) (KBr) spectrum of 3-methylpyrazolone **A**



SCHEME 4 Proposed mechanism for  $\text{Fe}_3\text{O}_4\text{@NAC}$ -catalyzed synthesis of THDPP1 from **A**

Besides, the analytical evidence confirmed the superiorities of both the catalyst-free and  $\text{Fe}_3\text{O}_4\text{@NAC}$ -catalyzed reaction in water by isolation of 97% yield of

intermediate **A** after 5 min. These results surprised us for no significant role of any catalyst in the formation of **A** in the first period of one-pot synthesis of THDPP1. With

melting point 222–224°C, FT-IR spectrum of 3-methylpyrazolone represented vibrational absorption modes at 3416 (NH stretching), 2889 (CH stretching), 1615 (overlapped-hydrogen-bonded amide-C=O stretching and C=N stretching), 1553 (NH bending), 1162 (C–N stretching), and 1015 (C–O stretching)  $\text{cm}^{-1}$  (Figure 9).

To evaluate the catalytic role of  $\text{Fe}_3\text{O}_4@\text{NAC}$  in the further steps, a different *p*-MCR was performed with the **A**,  $\text{NH}_4\text{OAc}$ , and benzaldehyde (2:1:1) in water without or with the optimal catalyst  $\text{Fe}_3\text{O}_4@\text{NAC}$  (12 mg) at room temperature. The 46% lower yield of THDPP1 after 60 min for a reaction run without catalyst versus 97% yield after 5 min for the  $\text{Fe}_3\text{O}_4@\text{NAC}$ -catalyzed experiment describes the requirement of catalyst in further reaction steps. Although we could not separate the highly active transients and unstable intermediates formed in further reaction steps, the following roles are proposed for the catalyst  $\text{Fe}_3\text{O}_4@\text{NAC}$  in the reaction mechanism (Scheme 4).

### 3.5 | Metal leaching, hot filtration, and recycling experiments

The ICP analysis conducted to test for leaching and entering the iron ions to the reaction mixture for the filtrate solution of fresh  $\text{Fe}_3\text{O}_4@\text{NAC}$  detected no trace of  $\text{Fe}^{+2}/\text{Fe}^{+3}$  in filtrate and confirmed no passing of them through the NAC-shell membrane during the filtration step.

For reusability test, after completion of the  $\text{Fe}_3\text{O}_4@\text{NAC}$ -catalyzed synthesis of THDPP1 from **A** in 10-mmol scale, hot ethanol was added, and nanocatalyst was collected by a magnet, washed with acetone, dried at 80°C, and reused in further four consecutive cycles. The only 4% decrease in yield at the constant time (5 min) after the fifth reaction run reveals a little catalytic activity loss (Figure 10). An analogous ICP analysis was performed for the filtrate solution of the reused  $\text{Fe}_3\text{O}_4@\text{NAC}$  after the fourth run to check the possible leaching of iron ions from the recycled catalyst. Once again no detection of iron showed no passing of  $\text{Fe}^{+2}/\text{Fe}^{+3}$  from the cellulosic-shell during reusing processes.

To check the heterogeneity of catalyst and leaching of NAC, a hot filtration test<sup>[40]</sup> was done for the  $\text{Fe}_3\text{O}_4@\text{NAC}$ -catalyzed typical *p*-MC synthesis of THDPP1 from the **A** by its separation with a magnet after 50% reaction progress (2 min) and keeping the mixture without the catalyst under similar conditions. No progress of the reaction showed heterogeneously

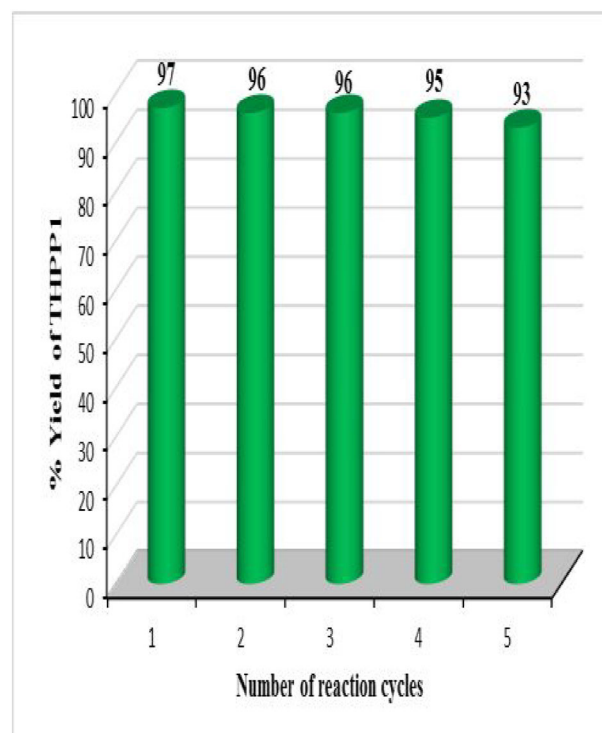


FIGURE 10 Reusability of the  $\text{Fe}_3\text{O}_4@\text{NAC}$  for the synthesis of THDPP1 from **A**

proceeding, while repeating a comparable hot filtration test for the reused catalyst after the fourth reaction run gave identical results for the fresh catalyst. Based on the BET analysis for the recovered  $\text{Fe}_3\text{O}_4@\text{NAC}$  after the fourth run, the specific surface, total pore volume, and mean pore diameter were  $14.08 \text{ m}^2 \text{ g}^{-1}$ ,  $0.029 \text{ cm}^3 \text{ g}^{-1}$ , and 9.97 nm and in agreements with the fresh catalyst amounts ( $14.10 \text{ m}^2 \text{ g}^{-1}$ ,  $0.030 \text{ cm}^3 \text{ g}^{-1}$ , and 9.96 nm, respectively). To find the more reliable results for stability of  $\text{Fe}_3\text{O}_4@\text{NAC}$ , the FT-IR, XRD, FESEM, and TEM techniques were employed to analyze the recovered catalyst  $\text{Fe}_3\text{O}_4@\text{NAC}$  after the fourth run (Figure 11).

As results from the ICP, hot filtration test, BET, TEM, FT-IR, FESEM, and XRD analyses for the recovered immobilized NAC on  $\text{Fe}_3\text{O}_4$  display,  $\text{Fe}_3\text{O}_4@\text{NAC}$  is a highly stable organometallic base catalyst.

The versatility of the heterogeneous and magnetic base catalyst  $\text{Fe}_3\text{O}_4@\text{NAC}$  was then demonstrated in the base-catalysis synthesis of the THDPPs from the intermediate **A**, an aldehyde, and  $\text{NH}_4\text{OAc}$  in water at room temperature (Table 2).

As results demonstrate, in general, a range of aldehydes could undergo rapid reactions with **A** and  $\text{NH}_4\text{OAc}$  to give the THDPPs in high yields.

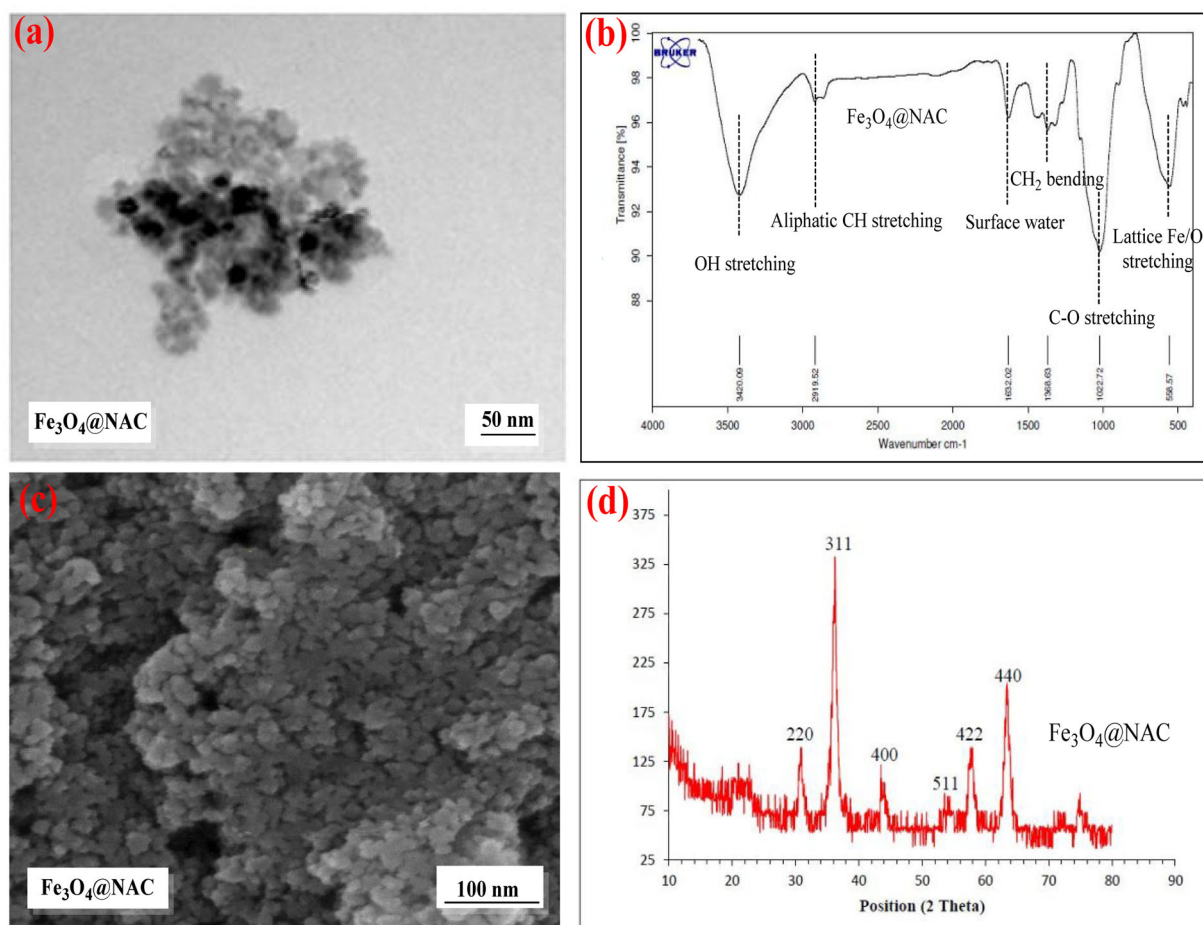


FIGURE 11 The transmission electron microscopy (TEM) (a), Fourier transform infrared (FT-IR) (b), field-emission scanning electron microscopy (FESEM) (c), and X-ray diffraction (XRD) (d) analyses for the recovered  $\text{Fe}_3\text{O}_4\text{@NAC}$  after the fourth run

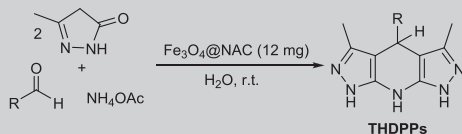


TABLE 2 The  $\text{Fe}_3\text{O}_4\text{@NAC}$ -catalyzed *p*-MCR for synthesis of THDPPs from **A**

Entry	R	Product	Time (min)	Yield (%)	Melting point (°C) found (reported) <sup>[31,36]</sup>
1	$\text{C}_6\text{H}_5$	THDDP1	5	97	240–242 (239–241)
2	$4\text{-Me}_2\text{NC}_6\text{H}_4$	THDDP2	7	97	241–243 (242–244)
3	$4\text{-MeC}_6\text{H}_4$	THDDP3	8	94	245–247 (244–246)
4	$4\text{-BrC}_6\text{H}_4$	THDDP4	15	88	163–165 (165–167)
5	$4\text{-ClC}_6\text{H}_4$	THDDP5	10	96	252–254 (254–256)
6	$2\text{-ClC}_6\text{H}_4$	THDDP6	10	91	221–223 (220–220)
7	$4\text{-HOC}_6\text{H}_4$	THDDP7	12	93	265–267 (265–267)
8	$4\text{-O}_2\text{NC}_6\text{H}_4$	THDDP8	7	96	235–237 (333–335)
9	$3\text{-O}_2\text{NC}_6\text{H}_4$	THDDP9	10	95	285–287 (285–286)

## 4 | CONCLUSIONS

The eco-biocompatible core-shell  $\text{Fe}_3\text{O}_4$ @nanoalkaline cellulose (NAC) was prepared by coagulation of cotton-derived NAC on the co-precipitated nano $\text{Fe}_3\text{O}_4$  at alkaline medium. The nano $\text{Fe}_3\text{O}_4$ @NAC nanoparticles in the range of 25–38 nm are slightly larger than  $\text{Fe}_3\text{O}_4$ , whereas the XRD pattern of  $\text{Fe}_3\text{O}_4$ @NAC shows similar crystallinity by  $\text{Fe}_3\text{O}_4$ . With a base capacity equal to 7.5-mmol  $\text{HO}^-/\text{g}$ , the VSM of  $\text{Fe}_3\text{O}_4$ @NAC displays magnetization saturation 35.2 emu/g. This thermally stable magnetic base catalyzes both of the water-based synthesis of THDPPs from hydrazine hydrate or 3-methylpyrazolone intermediate **A** by room temperature *p*-MCRs. While results suggest no need of catalyst in formation of the intermediate **A** as the first phase synthesis of THDPPs,  $\text{Fe}_3\text{O}_4$ @NAC has a clear catalytic performance in synthesis of THDPPs from the **A**. By this hybrid base catalyst, synthesis of THDPPs was achieved in the water at mild conditions with the advantages of high yielding at short reaction times, efficiency in low loading, and easy reusing of catalyst. Due to the stability of  $\text{Fe}_3\text{O}_4$ @NAC in leaching and hot filtration tests, it is a good candidate in water treatment and delivery of cationic biomaterials to targeted positions.

### ACKNOWLEDGMENT

The authors gratefully acknowledge partial support of this work by the Yazd University Research Council. This work is fully related to the PhD dissertation of Ehsan Ahmadi-AhmadAbadi from the Department of Chemistry of Yazd University under supervision of Prof. Fatemeh Tamaddon and advising of Dr. Hossein Kargar.

### CONFLICT OF INTEREST

All authors declare that they have no known conflict of interest, competing financial interests, or personal relationship that could have appeared to influence the work reported in this paper.

### AUTHOR CONTRIBUTIONS

**Fatemeh Tamaddon:** Conceptualization; project administration; supervision; validation. **Ehsan Ahmadi-AhmadAbadi:** Formal analysis; investigation; methodology; software; validation; visualization. **Hossein Kargar:** Formal analysis; validation; visualization.

### DATA AVAILABILITY STATEMENT

The additional data that support the findings of this paper are available in the supplementary material file of this article.

### ORCID

Fatemeh Tamaddon  <https://orcid.org/0000-0002-6686-8094>

Ehsan Ahmadi-AhmadAbadi  <https://orcid.org/0000-0001-7057-8201>

Hossein Kargar  <https://orcid.org/0000-0003-2319-0663>

### REFERENCES

- [1] A. Gennari, A. J. Führ, G. Volpato, C. F. V. de Soza, *Carbohydr. Polym.* **2020**, *1*, 246.
- [2] A. Nasiri, F. Tamaddon, M. H. Mosslemin, M. Amiri Gharaghani, A. Asadipour, *Environ. Health Eng. Manag.* **2019**, *6*, 41.
- [3] S. Sabaqian, F. Nemati, M. M. Heravi, H. T. Nahzomi, *Appl. Organomet. Chem.* **2017**, *1*, 31.
- [4] M. H. Beyki, M. Bayat, F. Shemirani, *Bioresour. Technol.* **2016**, *218*, 326.
- [5] X. An, D. Cheng, L. Dai, B. Wang, H. J. Ocampo, J. Nasrallah, X. Jia, J. Zou, Y. Long, Y. Ni, *Appl. Catal. B: Environ.* **2017**, *206*, 53.
- [6] J. Wei, Z. Yang, Y. Sun, C. Wang, G. Fan, G. Kang, R. Zhang, X. Dong, Y. Li, *J. Mater. Sci. Mater. Med.* **2019**, *54*, 6709.
- [7] T. Lindström, A. Naderi, A. Wiberg, *J. Korea TAPPI.* **2015**, *47*, 5.
- [8] L. R. Marcelo, J. Santos de Gois, A. Araujo da Silva, D. Vargas Cesar, *Environ. Chem. Lett.* **2020**, *18*, 1.
- [9] M. Islam, L. Chen, J. Sisler, K. Tam, *J. Mater. Chem. B* **2018**, *6*, 864.
- [10] K. Jedvert, T. Heinze, *J. Polym. Eng.* **2017**, *37*, 845.
- [11] N. Mahfoudhi, S. Boufi, *Cellulose* **2017**, *24*, 1171.
- [12] M. A. Ashraf, Z. Liu, C. Li, D. Zhang, *Appl. Organomet. Chem.* **2020**, *34*, 6133.
- [13] B. Gumina, F. Mauriello, R. Pietropaolo, S. Galvagno, C. Espro, *Mol. Catal.* **2018**, *446*, 152.
- [14] S. Azizi, J. Soleymani, M. Hasanzadeh, *Appl. Organomet. Chem.* **2020**, *34*, 5440.
- [15] I. A. Sacui, R. C. Nieuwendaal, D. J. Burnett, S. J. Stranick, M. Jorfi, C. Weder, E. J. Foster, R. T. Olsson, J. W. Gilman, *ACS Appl. Mater. Interfaces* **2014**, *6*, 6127.
- [16] S. Shojaei, Z. Ghasemi, A. Shahrisa, *Appl. Organomet. Chem.* **2017**, *31*, 3788.
- [17] J. Baruah, C. Chaliha, E. Kalita, B. K. Nath, R. A. Field, P. Deb, *Int. J. Biol. Macromol.* **2020**, *164*, 53.
- [18] P. A. Penttilä, A. Várnai, M. Fernández, I. Kontro, V. Liljeström, P. Lindner, M. Siika-aho, L. Viikari, R. Serimaa, *Cellulose* **2013**, *20*, 1031.
- [19] A. Maleki, A. A. Jafari, S. Yousefi, *Carbohydr. Polym.* **2017**, *175*, 409.
- [20] F. Tamaddon, S. Hosseinzadeh, *Cellulose* **2018**, *25*, 5277.
- [21] F. Tamaddon, D. Arab, E. Ahmadi-AhmadAbadi, *Carbohydr. Polym.* **2020**, *229*, 115471.
- [22] F. Tamaddon, M. T. Kazemi-Varnamkhashti, *Curr Catal.* **2017**, *6*, 57.
- [23] F. Tamaddon, D. Arab, *Int. J. Biol. Macromol.* **2019**, *134*, 1.
- [24] Y. T. Tao, C. H. Chuen, C. W. Ko, J. W. Peng, *Chem. Mater.* **2002**, *14*, 4256.
- [25] U. H. Manjunatha, S. Vinayak, J. A. Zambriski, A. T. Chao, T. Sy, C. G. Noble, G. M. C. Bonamy, R. R. Kondreddi, B. Zou, P. Gedeck, C. F. Brooks, G. T. Herbert, A. Sateriale, J. Tandel, S.

- Noh, S. B. Lakshminarayana, S. H. Lim, L. B. Goodman, C. Bodenreider, G. Feng, L. Zhang, F. Blasco, J. Wagner, F. J. Leong, B. Striepen, T. T. Diagana, *Nature* **2017**, *546*, 376.
- [26] A. Hantzsch, *Ber. Dtsch. Chem. Ges.* **1881**, *14*, 1637.
- [27] K. Zhao, M. Lei, L. Ma, L. Hu, *Monatsh. Chem.* **2011**, *142*, 1169.
- [28] M. Dabiri, P. Salehi, M. Koohshari, Z. Hajizadeh, D. I. MaGeec, *ARKIVOC* **2014**, *4*, 204.
- [29] S. K. Salama, A. F. Darweesh, I. A. Abdelhamid, A. H. Elwahy, *Polycyclic Aromat. Compd.* **2019**, *39*, 1.
- [30] S. M. Sadeghzadeh, *RSC Adv.* **2016**, *6*, 75973.
- [31] F. Tamaddon, A. Khorram, *J. Mol. Liq.* **2020**, *304*, 112722.
- [32] F. Tamaddon, D. Arab, *RSC Adv.* *19*(9), 41893.
- [33] F. Tamaddon, A. Khorram, *Synlett* **2020**, *31*, 691.
- [34] A. I. Vogel, B. S. Furniss, A. J. Hannaford, P. W. Smith, A. R. Tatchell, *Longman Scientific & Technical*, New York **1989**.
- [35] S. Vanegas, D. Rodriguez, C. Ochoa-Puentes, *ChemistrySelect* **2019**, *4*, 1.
- [36] N. G. Shabalala, R. Pagadala, S. B. Jonnalagadda, *Ultrason. Sonochem.* **2015**, *27*, 423.
- [37] M. Dashteh, M. Yarie, M. A. Zolfigol, A. Khazaei, S. Makhdoomi, *Appl. Organomet. Chem.* **2021**, *35*, e6222.
- [38] J. Safaei-Ghomi, H. Shahbazi-Alavi, R. Sadeghzadeh, A. Ziarati, *Res. Chem. Intermed.* **2016**, *42*, 8143.
- [39] L. Knorr, *Ber. Dtsch. Chem. Ges.* **1883**, *16*, 2597.
- [40] H. Lempers, R. Sheldon, *J. Catal.* **1998**, *175*, 62.

## SUPPORTING INFORMATION

Additional supporting information may be found online in the Supporting Information section at the end of this article.

**How to cite this article:** F. Tamaddon, E. Ahmadi-AhmadAbadi, H. Kargar, *Appl Organomet Chem* **2021**, e6386. <https://doi.org/10.1002/aoc.6386>